



Corrosion behavior of $\text{Al}_2\text{O}_3\text{-C}$ bricks in MnO-containing mold slag

Yi-jiang Zhao¹ · Guang-qiang Li^{1,2,3} · Yang Wu¹ · Cheng Yuan² · Ze Meng³ · Xiao-xuan Deng⁴ · Yu Liu¹

Received: 16 April 2023 / Revised: 5 June 2023 / Accepted: 7 June 2023 / Published online: 16 August 2023
© China Iron and Steel Research Institute Group Co., Ltd. 2023

Abstract

In order to explore the corrosion mechanism of $\text{Al}_2\text{O}_3\text{-C}$ refractories in the mold flux bearing MnO, the immersion test of $\text{Al}_2\text{O}_3\text{-C}$ refractories in $\text{CaO-SiO}_2\text{-CaF}_2\text{-MnO}$ slag with different MnO contents was carried out at 1550 °C. The results show that Mn particles were observed in the slag after experiment, due to the reduction of MnO by graphite in refractories. Large amounts of graphite were observed at the interface between refractories and slag, indicating that the oxidation of graphite is limited by the poor contact between graphite and molten slag. Therefore, the oxidation of graphite is not the main cause of damage to refractories. A small quantity of $\text{CaO}\cdot 2\text{Al}_2\text{O}_3$ (CA_2) and $\text{CaO}\cdot 6\text{Al}_2\text{O}_3$ (CA_6) adjacent to Al_2O_3 grain was detected at the slag/reaction layer interface. CA_2 and CA_6 possess relatively high melting points, which is beneficial to hindering the further penetration of slag. However, the dissolution of Al_2O_3 into slag is still the main cause for refractories damage. The increase in the MnO content of mold slag decreases the viscosity and then results in the severe corrosion of $\text{Al}_2\text{O}_3\text{-C}$ bricks.

Keywords $\text{Al}_2\text{O}_3\text{-C}$ refractory · MnO-containing slag · Graphite · Corrosion

1 Introduction

Oxide-based refractories are widely used in the steelmaking industrial production, due to the excellent mechanical properties and thermal shock resistance [1–4]. The submerged entry nozzle (SEN) composed of $\text{Al}_2\text{O}_3\text{-C}$ -based refractories plays an important role in preventing secondary oxidation of molten steel, controlling the flow rate of molten steel, and reducing slag entrapment in the continuous casting process [3–5]. However, the long-term

contact between SEN and mold fluxes can lead to the erosion and damage of SEN, which will hinder the smooth operation of continuous casting process and reduce production efficiency. Therefore, it is significant to study the erosion mechanism of $\text{Al}_2\text{O}_3\text{-C}$ -based refractories in slag.

The erosion mechanism of refractories in slag attracts widespread attentions, including the dissolution of refractories components into slag, the penetration of slag into refractories, and new phases formation by the reaction between slag and refractories [6–9]. Especially, the penetration of slag into refractories can deteriorate the thermal shock resistance and mechanical properties of refractories and accelerate the damage to refractories [10, 11]. Therefore, inhibiting the penetration of slag into refractories is beneficial to reducing the corrosion of refractories. The refractories bearing graphite possess excellent slag penetration resistance due to the poor wettability of slag and graphite [12–14]. However, the oxidation of carbon in refractories by slag components also causes the concerns about increased corrosion of refractories [15]. Moreover, the viscosity of slag is also an important factor affecting the dissolution of refractory components into slag and the penetration of slag into refractories [14, 15].

✉ Yu Liu
liuyu629@wust.edu.cn

¹ The State Key Laboratory of Refractories and Metallurgy, Wuhan University of Science and Technology, Wuhan 430081, Hubei, China

² Key Laboratory for Ferrous Metallurgy and Resources Utilization of Ministry of Education, Wuhan University of Science and Technology, Wuhan 430081, Hubei, China

³ Hubei Provincial Key Laboratory for New Processes of Ironmaking and Steelmaking, Wuhan University of Science and Technology, Wuhan 430081, Hubei, China

⁴ Research Institute of Technology, Shougang Group Co., Ltd., Beijing 100043, China

The traditional mold slag is mainly composed of CaO and SiO₂ as the base component, with an appropriate amount of CaF₂ and other fluxes. Furthermore, during the casting of the medium and high Mn steels, Mn in the molten steel will inevitably be oxidized and dissolved into slag, which increases the MnO content in slag [16]. It is well known that the graphite in refractories can be easily oxidized by MnO in molten slag, which could become the passage for slag penetration. In addition, MnO addition will decrease the slag viscosity [17], which would result in the severe corrosion of SEN. Therefore, it is significant to in-depth study the effect of MnO in mold slag on the corrosion of Al₂O₃-C-based refractories. However, to the authors' best knowledge, there is little research on the corrosion mechanism of Al₂O₃-C refractories in the mold slag bearing MnO. Therefore, the immersion experiment was carried out to study the interaction between molten slag bearing MnO and Al₂O₃-C refractories and the effect of MnO content in mold powders on the corrosion behavior of Al₂O₃-C refractories, aiming to provide the fundamental knowledge for the corrosion mechanism of Al₂O₃-C refractories in slag bearing MnO.

2 Experimental

2.1 Materials preparation

The Al₂O₃-C refractories were prepared with tabular alumina (< 0.075 mm, 0–1 mm, and 1–3 mm), α -Al₂O₃ (< 45 μ m), flake graphite (< 74 μ m, 97.5 wt.% C), and silicon powders (purity 98%; median diameter d_{50} = 27 μ m) as raw materials. Table 1 lists the chemical composition of main raw materials. Furthermore, the adhesive is thermosetting phenolic resin (36 wt.% C). After fully mixing, the raw materials were pressed into cuboid samples (150 mm \times 25 mm \times 25 mm) and then cured at 220 $^{\circ}$ C for 24 h. Afterwards, the cured samples were placed in a graphite crucible, covered with petroleum coke, heated to 1200 $^{\circ}$ C, and held for 3 h in an electric furnace under the argon atmosphere. It should be noted that the Al₂O₃-C refractories were prepared according to common process parameters. Furthermore, this study focuses on the effect of slag composition on the dissolution behavior of refractories.

Table 1 Compositions of Al₂O₃-C refractories samples (wt.%)

Tabular alumina			α -Al ₂ O ₃	Flake graphite	Silicon powder
1–3 mm	0–1 mm	< 0.075 mm			
40	30	9	8	10	3

The Al₂O₃-C refractories were machined into the cuboid samples with the dimension of 60 mm \times 12 mm \times 12 mm for the immersion corrosion experiment. It is well known that the CaF₂ significantly affects the slag viscosity. In order to elucidate the effect of MnO content in the slag on the slag viscosity, the CaF₂ addition content was kept constant in all experimental slag groups. The composition of mold slag containing MnO used for experiment is listed in Table 2. The liquidus temperature of slag samples was calculated using the thermodynamic calculation software FactSage 8.1. The liquidus temperature of slag samples decreases with the increase in MnO content. The tested slag was prepared using the reagent-grade powders of SiO₂, CaF₂, CaO, and MnO (Sinopharm Chemical Reagent Co., Ltd., China). In order to avoid the influence of other impurities in the powders, SiO₂ and CaF₂ powders were calcined at 300 $^{\circ}$ C, and CaO powders were calcined at 1000 $^{\circ}$ C for 10 h in the muffle furnace, respectively. The slag was premelted in a high-frequency induction furnace and quenched on the copper plate.

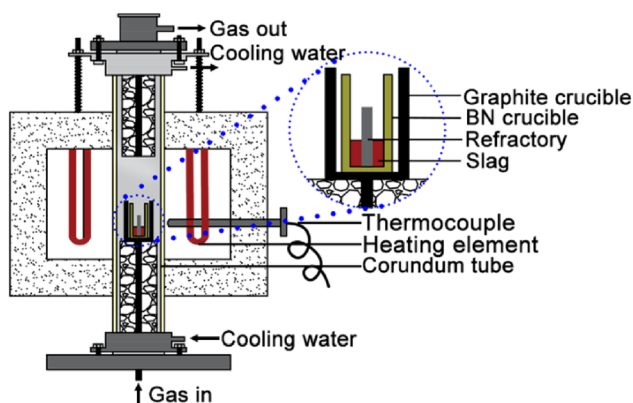
2.2 Experimental procedure

The experimental device is shown in Fig. 1. In order to avoid the effect of crucible corrosion, the boron nitride crucibles (inner diameter of 30 mm and height of 90 mm) were selected for the corrosion tests. Firstly, the slag (\sim 20 g) was put into the boron nitride crucible. Then, the boron nitride crucible was placed in a resistance furnace and heated to 1550 $^{\circ}$ C under the Ar atmosphere with the flow rate of 300 mL/min. After holding at 1550 $^{\circ}$ C for 30 min, the boron nitride crucible was removed from the furnace, and the sample was quenched on the copper plate. This procedure was repeated for other corrosion tests.

The obtained samples were enclosed in the epoxy resin for avoiding mechanical damage and cut from the middle of the samples for the microscopic observation of corrosion interface. The microstructure and composition of slag/refractories interface were analyzed using a scanning electron microscope (SEM, Nova 400 Nano, FEI Company, USA) equipped with an energy-dispersive spectrometer (EDS, NCA IE 350 Penta FET X-3, Oxford Company, UK). Besides, the contents of Al₂O₃ in the slag samples after corrosion were detected with an X-ray fluorescence spectrometer (XRF, ARL 9900 Series, USA).

Table 2 Chemical compositions and liquidus temperatures of experimental slags

Slag No.	Chemical composition/wt.%				Liquidus temperature/°C
	CaO	SiO ₂	CaF ₂	MnO	
S1	45	45	10	0	1412
S2	42.5	42.5	10	5	1361
S3	40	40	10	10	1306

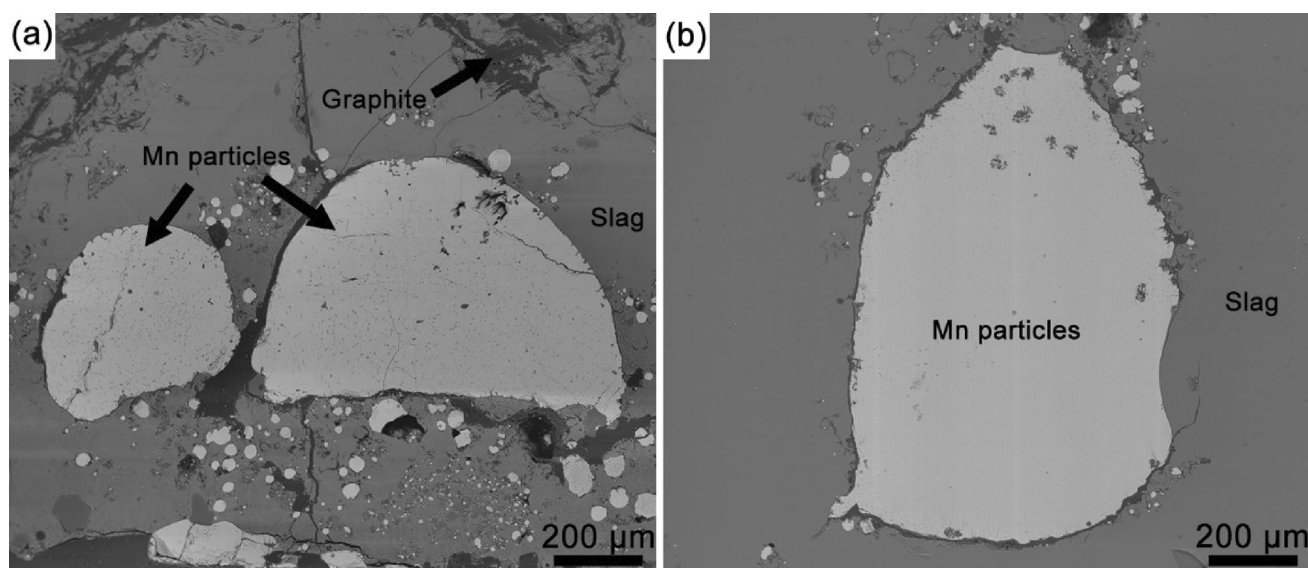
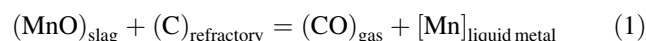
**Fig. 1** Schematic diagram of experimental device

3 Results and discussion

As shown in Fig. 2, the large Mn particles are found in the slag samples after experiment. The sizes of 13 large Mn particles were measured, and the largest equivalent diameter is 0.9 mm. It can be inferred that the Mn particles were formed by the interaction between molten slag and

refractories. Furthermore, the small Mn particle trends to aggregate and forms the large particle due to the interface tension difference between Mn and slag. Lots of small particles were observed around the large particles, which prove the aggregation of Mn particles.

Figure 3 shows the $\Delta G-P_{\text{CO}}/P^{\theta}$ diagram of chemical reactions between graphite and components in slag containing 10 wt.% MnO, where ΔG is the change of Gibbs free energy, and P_{CO}/P^{θ} is the partial pressure of CO in the mixed gas. The standard Gibbs free energy changes (ΔG^{θ} , J mol⁻¹) of reactions between graphite and MnO were calculated by the thermodynamic calculation software FactSage 8.1. The activities of slag components were also obtained by FactSage 8.1 and are listed in Table 3. It can be seen that under low P_{CO}/P^{θ} , reaction (1) can proceed. Under the conditions of this experiment, P_{CO}/P^{θ} can be maintained at a lower level due to the introduction of Ar gas (purity of 99.999 vol.%). It indicates that the Mn particles are formed mainly due to the reduction of MnO in slag by graphite in refractories, as shown in reaction (1) [18, 19]:

**Fig. 2** Large Mn particles in slag near interface. **a** Slag S2; **b** slag S3

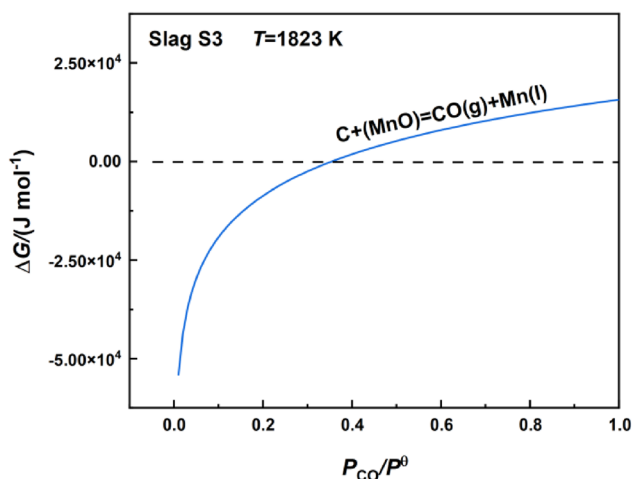


Fig. 3 $\Delta G-P_{CO}/P^0$ diagram of chemical reactions between C and MnO. T —Temperature

Figure 4 shows the microstructure and phase compositions of interface between slag and refractories after the corrosion tests. Lots of graphite were observed at the slag/refractories interface for all samples, indicating that the graphite in refractories was not completely oxidized by MnO in slag and remained at the interface during the corrosion tests. The elements mapping of interface between slag S3 and refractories is shown in Fig. 5. It indicates that Al₂O₃ inside the graphite was severely eroded by slag,

while the graphite was only slightly eroded by slag. The main reason for the above results is that the wettability between graphite and slag is poor, which hinders the penetration of slag into refractories and reduces graphite oxidation [18, 20].

Figure 6 shows the detailed phase composition of interface between slag S3 (10 wt.% MnO) and refractories. New phases are formed by the reaction between the penetrated slag and Al₂O₃ (Fig. 6b). The EDS results shown in Table 4 indicate that the particles in slag are composed of Al₂O₃-SiO₂-CaO (Fig. 6b), which has a relatively low melting point. The CaO percentage of liquid phases in varied local region along the slag penetration direction shows the decreasing trend (Table 4 and Fig. 6b). A small quantity of CaO·2Al₂O₃ (CA₂, melting point of 1780 °C) and CaO·6Al₂O₃ (CA₆, melting point of 1860 °C) adjacent to Al₂O₃ grain was detected at the slag/reaction layer interface. The formations of CA₂ and CA₆ phases with high melting point are beneficial to hindering the further penetration of slag [21–25]. However, the dissolution of Al₂O₃ into slag is still the main cause of refractories damage [26].

The Al₂O₃ contents in the slag samples after the corrosion tests are shown in Fig. 7. The Al₂O₃ content increases with the increase in MnO content in the slag. The result indicates that the increase in the MnO content in mold slag accelerates the dissolution of Al₂O₃-C bricks, leading to the increased corrosion of the bricks.

Table 3 Activities of slag components at 1550 °C

Slag No.	CaO	SiO ₂	CaF ₂	MnO	$\frac{a_{CaF_2}^3 \cdot a_{Al_2O_3}}{a_{CaO}^3}$	$a_{MnO} \cdot a_C$
S1	1.64×10^{-3}	0.1935	0.0859	–	1.44×10^5	–
S2	1.78×10^{-3}	0.1567	0.0965	0.0335	1.59×10^5	0.0335
S3	1.99×10^{-3}	0.1219	0.1092	0.0705	1.65×10^5	0.0705

a —Activity of component

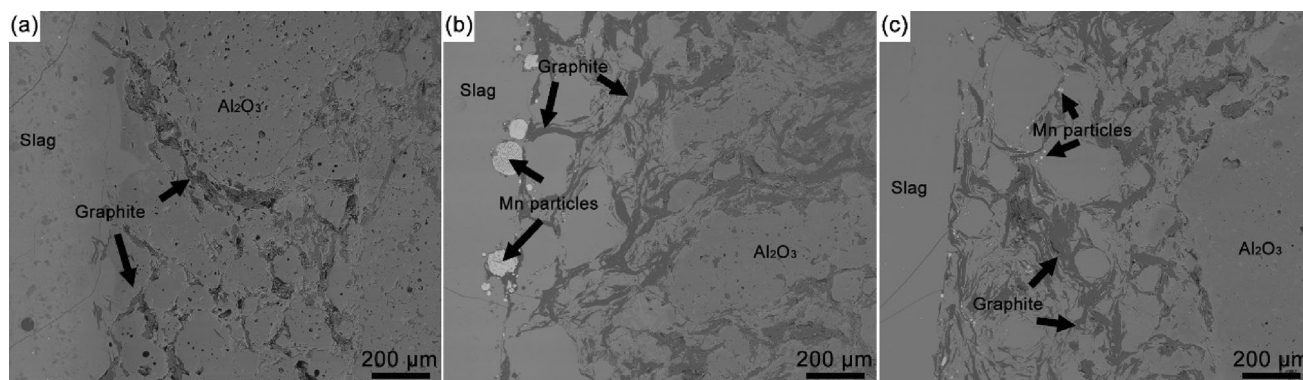


Fig. 4 Micrograph of slag/refractories interface of samples after corrosion experiment. **a** Slag S1; **b** slag S2; **c** slag S3

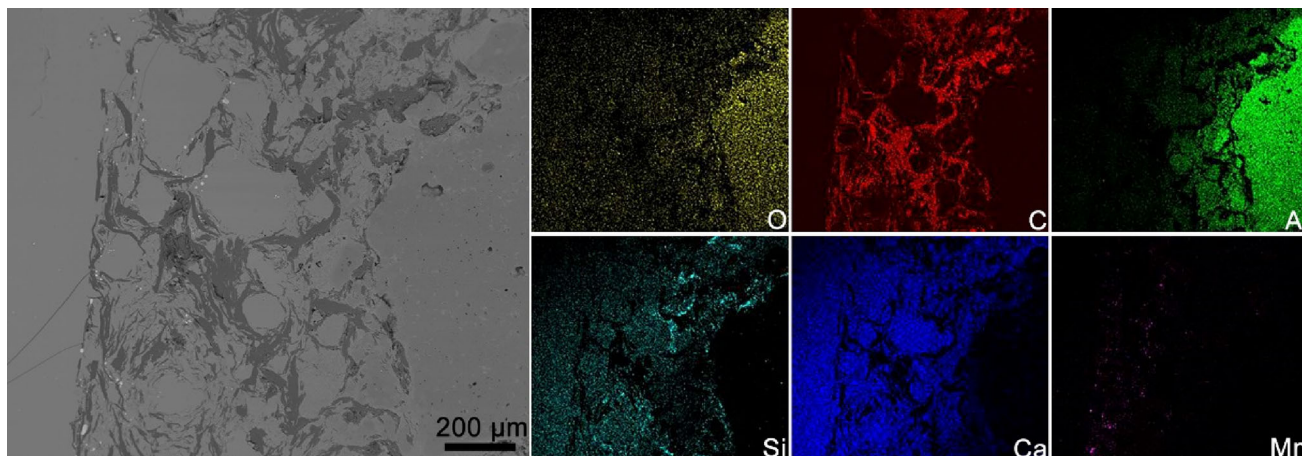


Fig. 5 EDS mapping of slag/refractories interface after corrosion for slag S3

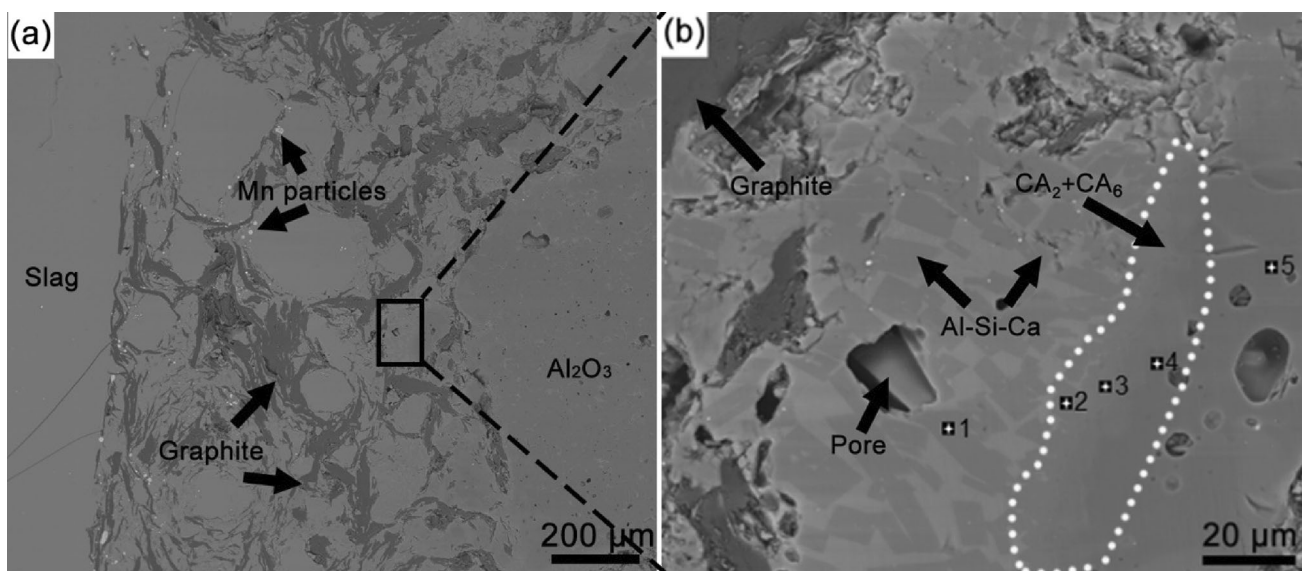


Fig. 6 Slag/refractories interface (a) and slag penetration in refractories (b) for slag S3 case. Al–Si–Ca is Al₂O₃–SiO₂–CaO low melting point phase

Table 4 EDS results of each point in Fig. 6 (at.%)

Element	Si	Ca	Al	O
Point 1	3.08	13.64	33.22	50.06
Point 2	0.67	11.91	39.17	48.25
Point 3	–	5.48	44.69	49.82
Point 4	–	4.78	45.48	49.74
Point 5	–	–	49.00	51.00

The properties of slag have an important impact on the corrosion behavior of refractories, especially the viscosity of slag [6, 27–30]. Figure 8 shows the viscosity change of initial slag samples with temperature calculated by Riboud model as follows [15]:

$$\eta = A \cdot T \exp\left(\frac{B}{T}\right) \tag{2}$$

$$A = \exp[-19.81 + 1.73(x_{CaO} + x_{MgO} + x_{FeO} + x_{MnO}) + 5.82x_{CaF_2} + 7.02(x_{Na_2O} + x_{K_2O}) - 35.76x_{Al_2O_3}] \tag{3}$$

$$B = 31,140 - 23,896(x_{CaO} + x_{MgO} + x_{FeO} + x_{MnO}) - 46,356x_{CaF_2} - 39,159(x_{Na_2O} + x_{K_2O}) + 68,833x_{Al_2O_3} \tag{4}$$

where η is the viscosity of slag, Pa s; and x is the mole fraction of a component. At the experimental temperature, the viscosities of slag samples (S2 and S3) containing MnO are both lower than that of the slag without MnO (S1), and the viscosity of slag decreases with the increase in MnO

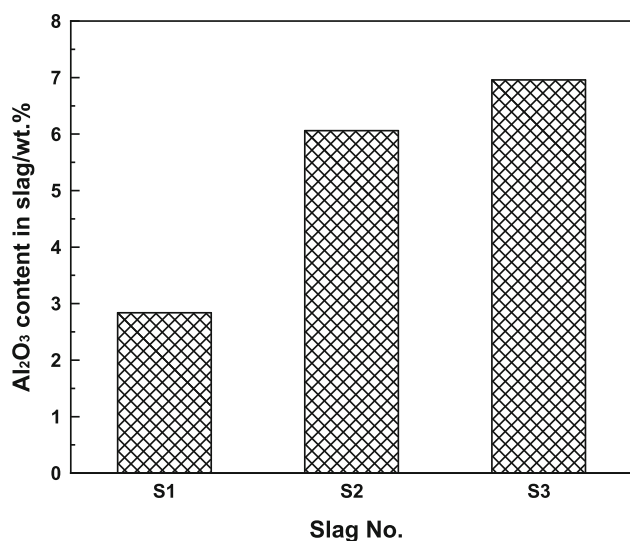


Fig. 7 Al₂O₃ content in slag after corrosion experiment

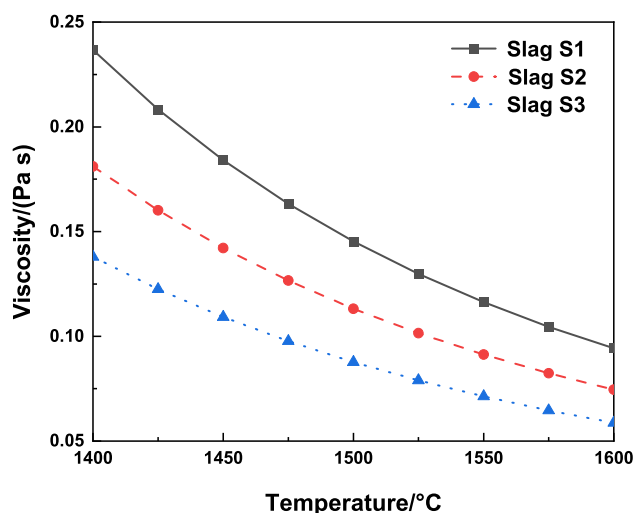


Fig. 8 Viscosity change of three groups of slags at different temperatures

content in slag. It is well known that the lower the viscosity of the slag, the more conducive to the penetration of the slag. The lower viscosity provides the better kinetic conditions for the slag penetration into refractories and the mass transfer in liquid phase. Therefore, the corrosion of Al₂O₃-C refractories in the slag S3 with higher MnO content is severer than that in the slag S2 with lower MnO content.

Although the oxidation of graphite is not the main cause for the deterioration of Al₂O₃-C bricks, the severer graphite oxidation is inevitably detrimental to the slag resistance of refractories. From the view of thermodynamics, the driving force for the graphite deoxidation by MnO

increases with the increase in MnO content in molten slag. Taking the pure substance as standard state, a_C in refractories is unity. The driving force of reaction (1) can be expressed by $a_{MnO} \cdot a_C$, as shown in Table 3. The value of $a_{MnO} \cdot a_C$ in the test of slag S3 is significantly larger than that in the test of slag S2. Compared with slag S2, reaction (1) occurs more easily in the test of slag S3. Therefore, the content of Al₂O₃ in slag increases with the increase in MnO content from 5 wt.% (slag S2) to 10 wt.% (slag S3).

Furthermore, the interaction between CaF₂ in slag and Al₂O₃ in refractories can also aggravate the corrosion of Al₂O₃-C refractories. The reaction is shown in reaction (5) [31]:

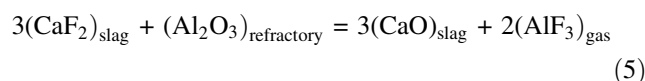


Table 3 shows that the activities of CaO and CaF₂ in slag increase as the content of MnO in slag increases [15]. The driving force of reaction (5) can be expressed by $\frac{a_{\text{CaF}_2}^3 \cdot a_{\text{Al}_2\text{O}_3}}{a_{\text{CaO}}^3}$. The driving force of reaction (5) for the slag containing MnO (S2 and S3) is larger than that free MnO slag S1, and the driving force increases with increase in MnO content in slag, especially for the slag S3 with higher MnO content. Therefore, the corrosion of Al₂O₃-C refractories in the slag containing MnO is severer than that in the slag without MnO, especially for the slag S3 with higher MnO content.

4 Conclusions

1. Mn particles are observed in the slag after experiment, which was resulted from the reduction of MnO by the graphite in Al₂O₃-C refractories.
2. A large amount of graphite is observed at the refractories/slag interface, indicating that the oxidation of graphite is limited by the poor wettability between graphite and molten slag, which is not the main cause for the deterioration of Al₂O₃-C bricks. It indicates that the dissolution of Al₂O₃ into slag is still the main cause of refractories damage.
3. The dissolution amount of Al₂O₃ increases with the increase in MnO content in slag, indicating that MnO-containing slag will result in the severe corrosion of SEN.

Acknowledgements The authors gratefully acknowledge the support from the National Natural Science Foundation of China (52274305 and U1860205) and Young Elite Scientists Sponsorship Program by CAST (2022QNRC001).

Declarations

Conflict of interest The authors declare that they have no known competing financial interest or personal relationships that could have appeared to influence the work reported in this paper.

References

- [1] Y. Chen, G. Liu, X. Hou, F. Yang, B. Fan, R. Zhang, H. Li, *Ceram. Int.* 43 (2017) 14599–14607.
- [2] Y. Liu, W. Yan, Z. Chen, J. Chen, Y. Liu, G. Li, *J. Eur. Ceram. Soc.* 43 (2023) 3794–3803.
- [3] J. Zhang, X. Li, W. Gong, P. Chen, B. Zhu, *J. Eur. Ceram. Soc.* 39 (2019) 2739–2747.
- [4] C. Atzenhofer, S. Gschiel, H. Harmuth, *J. Eur. Ceram. Soc.* 37 (2017) 1805–1810.
- [5] M. Long, X. Zuo, L. Zhang, D. Chen, *ISIJ Int.* 50 (2010) 712–720.
- [6] J. Song, Y. Liu, X. Lv, Z. You, *J. Mater. Res. Technol.* 9 (2020) 314–321.
- [7] W. Wang, L. Xue, T. Zhang, L. Zhou, J. Chen, Z. Pan, *Ceram. Int.* 45 (2019) 20664–20673.
- [8] J. Liu, Z. Liu, J. Feng, B. Li, J. Chen, B. Ren, Y. Jia, S. Yin, *Materials* 15 (2022) 6779.
- [9] A. Kumar, R. Khanna, M. Ikram-ul-Haq, J. Spink, V. Sahajwalla, *Steel Res. Int.* 87 (2016) 46–56.
- [10] W.E. Lee, S. Zhang, *Int. Mater. Rev.* 44 (1999) 77–104.
- [11] B. Ma, Q. Zhu, Y. Sun, J. Yu, Y. Li, *J. Mater. Sci. Technol.* 26 (2010) 715–720.
- [12] S. Taira, K. Nakashima, K. Mori, *ISIJ Int.* 33 (1993) 116–123.
- [13] W.D. Cho, P. Fan, *ISIJ Int.* 44 (2004) 229–234.
- [14] J.Y. Choi, H.G. Lee, J.S. Kim, *ISIJ Int.* 42 (2002) 852–860.
- [15] Y. Liu, J. Rao, G. Li, Z. Zhang, J. Wang, T. Dong, *Ceram. Int.* 48 (2022) 19068–19072.
- [16] L. Kong, Z. Deng, L. Cheng, M. Zhu, *Metall. Mater. Trans. B* 49 (2018) 3522–3533.
- [17] H.B. Zuo, C. Wang, C.F. Xu, J.L. Zhang, T. Zhang, *Ironmak. Steelmak.* 43 (2016) 56–63.
- [18] Y. Liu, Q. Wang, G. Li, J. Zhang, W. Yan, A. Huang, *Ceram. Int.* 46 (2020) 7517–7522.
- [19] D. Xie, C. Garlick, T. Tran, *ISIJ Int.* 45 (2005) 175–182.
- [20] M.A. Van Ende, M. Guo, P.T. Jones, B. Blanpain, P. Wollants, *Ceram. Int.* 35 (2009) 2203–2212.
- [21] Y. Liu, E. Wang, L. Xu, T. Yang, Z. He, T. Liang, X. Hou, *Int. J. Miner. Metall. Mater.* 30 (2023) 756–765.
- [22] C. Guo, E. Wang, X. Hou, J. Kang, T. Yang, T. Liang, G. Bei, *J. Am. Ceram. Soc.* 104 (2021) 4854–4866.
- [23] E.H. Wang, C. Luo, J.H. Chen, X.M. Hou, *J. Iron Steel Res. Int.* 27 (2020) 169–179.
- [24] A.G. Tomba Martinez, A.P. Luz, M.A.L. Braulio, V.C. Pandolfelli, *Ceram. Int.* 41 (2015) 4714–4725.
- [25] J. Chen, L. Chen, Y. Wei, N. Li, S. Zhang, *Corros. Sci.* 143 (2018) 166–176.
- [26] C. Xuan, W. Mu, *J. Am. Ceram. Soc.* 104 (2021) 57–75.
- [27] J. Liu, F. Verhaeghe, M. Guo, B. Blanpain, P. Wollants, *J. Am. Ceram. Soc.* 90 (2007) 3818–3824.
- [28] R. Xu, J. Zhang, Z. Li, Y. Zhao, *ISIJ Int.* 59 (2019) 1933–1939.
- [29] J.H. Park, M.O. Suk, I.H. Jung, M. Guo, B. Blanpain, *Steel Res. Int.* 81 (2010) 860–868.
- [30] Y. Liu, Y. Wang, G. Li, C. Yuan, R. Lu, B. Li, *J. Therm. Anal. Calorim.* 139 (2020) 923–931.
- [31] Y. Liu, Z. Zhang, G. Li, Y. Wu, D. Xu, B. Li, *Vacuum* 158 (2018) 6–13.

Springer Nature or its licensor (e.g. a society or other partner) holds exclusive rights to this article under a publishing agreement with the author(s) or other rightsholder(s); author self-archiving of the accepted manuscript version of this article is solely governed by the terms of such publishing agreement and applicable law.